# EMRP SIB05 NewKILO – Summary report of Work Package 3

Deliverables 3.3.1, 3.4.1 & 3.4.2

## *Surface effects and dynamic changes on the artefact surface between vacuum, air and selected gases*

Peter Fuchs (EJPD), Kilian Marti (EJPD), James Berry (NPL), Michael Borys (PTB), Stuart Davidson (NPL), Richard Green (NRC), Richard Hogstrom (MIKES), Sevda Kacmaz (TUBITAK), Andrea Malengo (INRIM), Paul-André Meury (LNE), Matthias Müller (PTB), Andreas Nutsch (PTB), Zaccaria Silvestri (CNAM), Jaroslav Zuda (CMI).

## Contents

# 1 Introduction

The aim of this work package is to use a range of complementary surface analysis techniques to characterize the surface effects on artefacts stored in and transferred between air, vacuum and inert gas and to facilitate the development in WP2 of optimal transfer methods for minimal sorption.

# 2 Experimental

The surface samples were manufactured within WP1 and sent to the WP leader METAS. Details about the preparation are summarized in the Reports of WP1. At METAS, NPL and TUBITAK all samples were examined by XPS for surface chemical analysis. The different samples distributed to NMIs are listed below. For the studies at CNAM large 5 cm in diameter and very flat samples were needed. Therefore CNAM prepared their own samples.

| Sample/NMI | NPL | CNAM | CMI | EJPD | PTB | MIKES | TUBITAK | Total |
|---|---|---|---|---|---|---|---|---|
| **PtIr** | 3 | 1 | | 3 | 3 | 3 | | **13** |
| **AuPt** | 3 | | 3 | 3 | 3 | | | **12** |
| **Ir** | 3 | | | 3 | 3 | 3 | | **12** |
| **SS** | | 1 | 3 | | | 3 | 3 | **10** |
| **Si** | 3 | | 3 | | 3 | | | **9** |
| **W (single)** | 3 | | | 3 | 3 | 3 | | **12** |
| **Ni alloy** | 3 | | 3 | | | | 3 | **9** |
| **Au (ep)** | | | 3 | 3 | | 3 | 3 | **12** |
| **Rh (ep)** | | | 3 | 3 | | 3 | 3 | **12** |
| **Total** | **18** | **2** | **18** | **18** | **15** | **18** | **12** | **101** |

Table 1: Sample distribution among the JRP-partners.

# 3 Results

## 3.1 Initial surface layer composition

As received the samples were analyzed by XPS (METAS, NPL, TUBITAK), XRF (PTB) and TDS (CNAM). Besides the bulk materials, a natural contamination by C and O compounds was found. Surprisingly, on almost all samples traces of other contaminants mainly up to 1% of Cu was identified. The origin of these Cu traces is not clear. A potential source of contamination is the wet polishing process when Cu or Cu-alloys are in contact with the polishing liquid [1-3]. Additionally, TUBITAK found traces of Sulfur on Rh and PTB identified traces of Ru on PtIr and Ir. The other participants did not detect these elements on their samples.

| PtIr<br>7+8 | AuPt<br>10+11 | Ir<br>7+8 | Si<br>7+9 | W<br>7+8 |
|---|---|---|---|---|
| C (Kα) | - | C (Kα) | C (Kα) | - |
| N(Kα) | - | | | N (Kα) |
| O(Kα) | O (Kα) | - | O (Kα) | O (Kα) |
| - | - | | F (Kα) | - |
| Mg (Kα) | - | - | - | Mg (Kα) |
| Al (Kα) | Al (Kα) | - | Al (Kα) | Al (Kα) |
| - | - | - | - | - |
| - | - | Ca (Kα) | - | - |
| Fe (Kα) | Fe (Kα) | Fe (Kα) | Fe (Kα) | Fe (Kα) |
| Ni (Kα) | - | Ni (Kα) | Ni (Kα) | Ni (Kα) |
| Cu (Lα & Kα) | Cu (Kα) | Cu (Kα) | Cu (Lα+Kα) | Cu (Kα) |
| Zn (Lα & Kα) | - | Zn (Kα) | - | Zn (Kα) |
| Ru (Mz & Lα) | - | Ru (Mz & Lα) | - | - |
| Ag (Lα) | Ag (M & Lα) | - | - | - |

Table 2: Identified trace elements derived from XRF spectra (data from PTB). For the trace elements marked in yellow, high fluorescence intensities have been found.

## 3.2 Cyclic exposures to air

The samples were cycled between vacuum and air and were subsequently analyzed by different surface analysis techniques such as XPS, XRR and TDS. This sequence of measurements was repeated and carried out for different initial conditions:

1) As received from METAS (after ultrasonic cleaning with solvents and storage in air for 6 weeks)
2) After cleaning with H-Plasma (@ 0.7 mbar H-pressure, cleaning time = 30 minutes)
3) After cleaning with UV/ozone (@ NPL: UV radiation at sample position = 13 mW $cm^{-2}$, $O_3$ concentration = 115 ppm; @ Metas: UV radiation at the sample position = 8 mW $cm^{-2}$, $O_3$ concentration = 43 ppm)
4) After cleaning with nettoyage-lavage, here usually referred to as the BIPM procedure as described in [4].

The result from NPL for the thickness of the H-C layer on PtIr and Si as received and after 3 different cleaning procedures is depicted in Figure 1. At NPL UV cleaning was found to be best for the removal of H-C compounds followed by hydrogen plasma, whereas nettoyage-lavage increases the contamination. Right after the cleaning, the results from METAS (first point in Figure 2) exhibit a different behaviour. For all materials the cleaning by hydrogen plasma at METAS was most effective, followed by UV cleaning and the nettoyage-lavage, except for AuPt where the nettoyage-lavage was slightly better. In contrast to the NPL results no increase of the initial contamination after nettoyage-lavage was found. The discrepant results of the two laboratories may be caused by differences in the procedures: con-

centration of ozone and H+, operator (nettoyage-lavage [4]), time elapsed between cleaning and analysis etc. However, UV/$O_3$ and H-plasma clearly reduce hydrocarbons, while the nettoyage-lavage leads to controversial results which are most likely due to the dependence on the operator.

At this point we note that the result from H-plasma cleaning depend on the base pressure of the plasma reactor. In case of bad base pressure also molecules other than hydrogen are present. These molecules are also ionized and do react. Consequently, several processes with different process gases are superimposed and run in parallel.

The thickness of the hydrocarbon contamination on the surface of the PtIr and silicon samples has been calculated by NPL and METAS using the following formula taken from a paper by Graham Smith [5]:

$$d = -\lambda_{C1s,C} \cos\theta \ln\left(1 - \frac{x}{100}\right) \tag{3.1}$$

where $x$ = atomic %

$\lambda_{C1s,C}$ = the effective electron attenuation length for carbon 1s photoelectrons in the hydrocarbon overlayer

The effective electron attenuation length for carbon 1s photoelectrons in the hydrocarbon overlayer ($\lambda_{C1s,C}$) has been calculated from the following formula derived by Seah and Spencer [6] for an average organic overlayer:

$$\lambda_{C1s,C} = 0.00837E^{0.842} \tag{3.2}$$

where $E$ is the kinetic energy of the peak of interest.

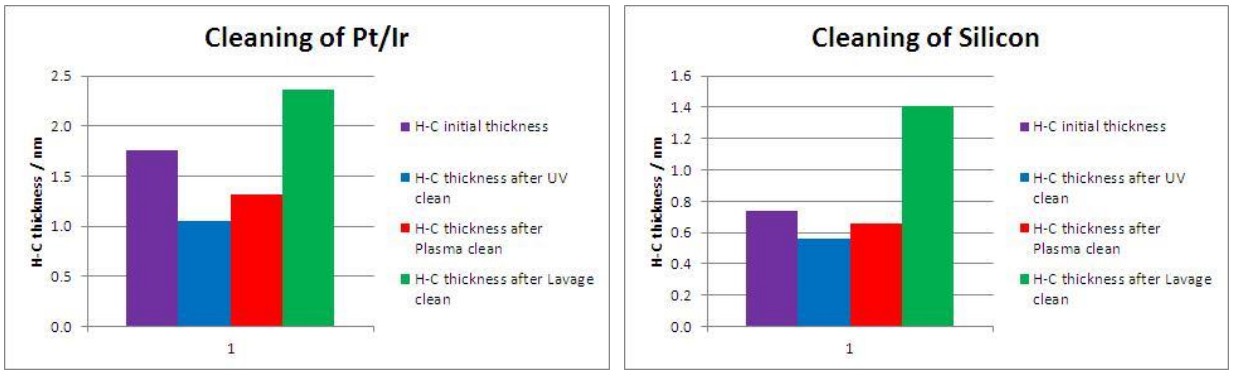


Figure 1: H-C layer thickness on PtIr and Si as received and after cleaning by different procedures (data from NPL).

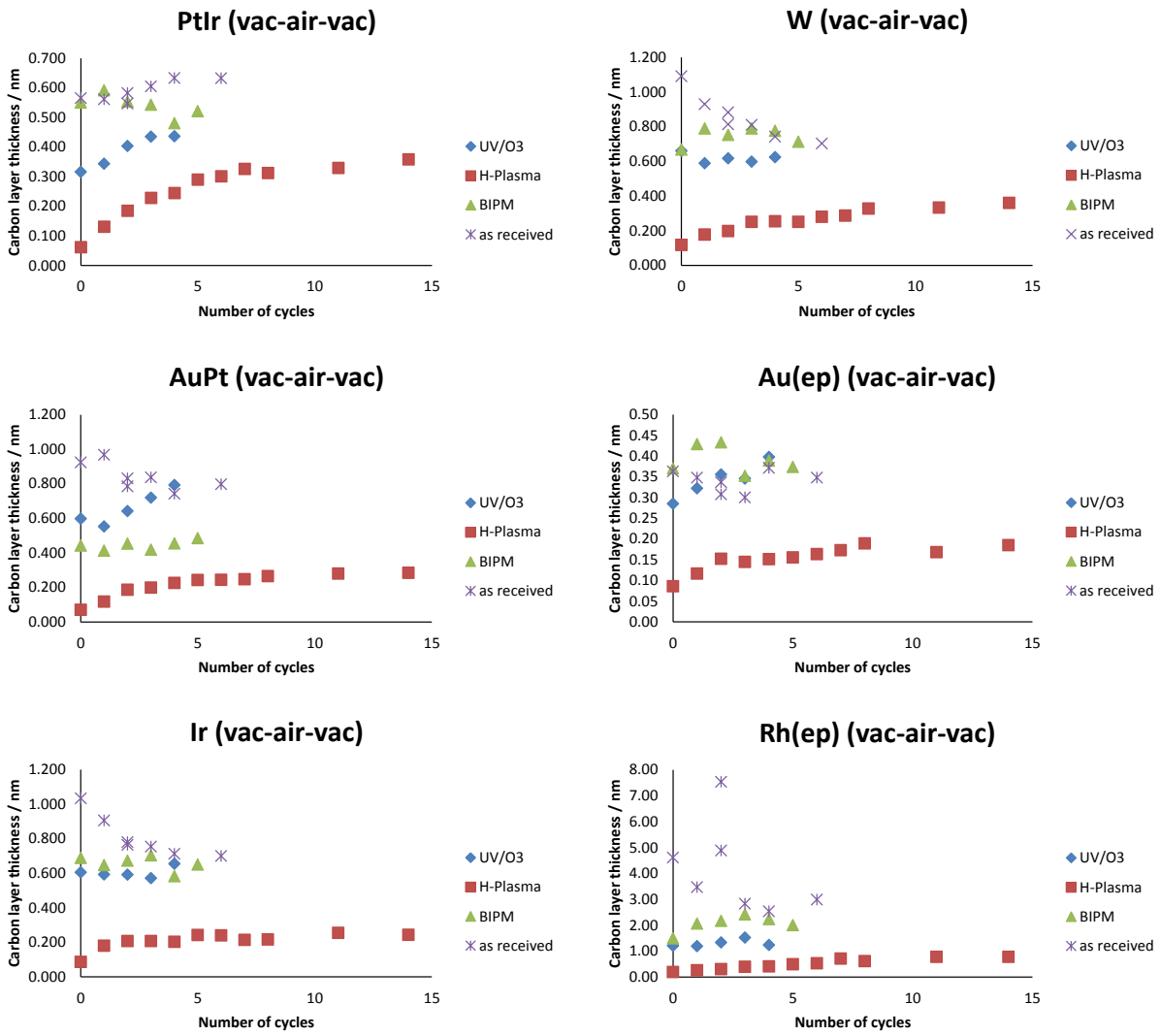


Figure 2: Overlayer thickness of carbon calculated from XPS intensities as a function of vac-air-vac cycles for different initial conditions (data from METAS).

Figure 2 shows the change in the overlayer thickness of carbon with increasing number of vacuum-air-vacuum cycles. In the as-received state, the contamination on all samples except on PtIr was slightly reduced by cyclic venting to air. We attribute this to the desorption of loosely bonded C-compounds when exposed to vacuum. The desorption is highest for W and Ir. In contrast, the contamination for PtIr increased slightly.

After UV/ozone cleaning the initial contamination is reduced, but did not remarkably change with exposures to air, except for Au and AuPt. As we will show later this is due to the decomposition of gold oxides rather than an increase in contamination.

H-plasma significantly reduces the contamination. Upon exposures to air the contamination by hydrocarbons is at first very fast, but slows down rapidly. After 5-10 venting cycles the contamination saturates at roughly the same level as for the UV/ozone cleaned samples.

A comparison of the above results is summarized in Figure 3a for the normalized C-intensities and in Figure 3b for the calculated layer thicknesses. The corresponding ranking lists for the best materials and best processes are given in Table 3 and Table 4.

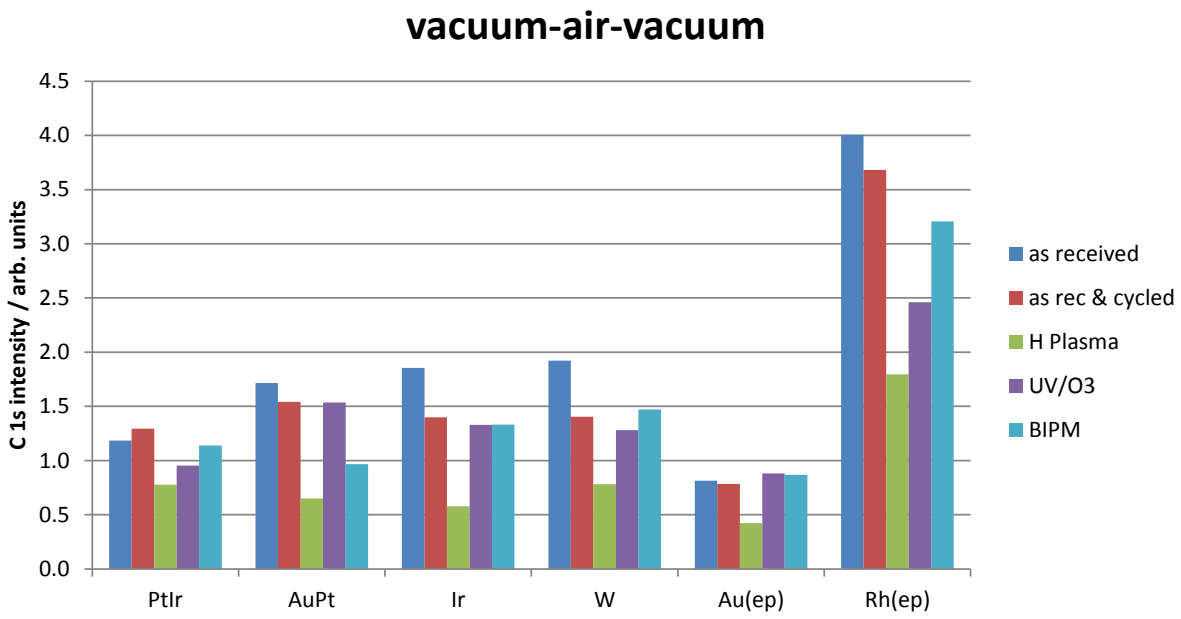


Figure 3a: Final carbon intensities (normalized) for different materials as received (dark blue) and after cyclic venting directly to air for different initial conditions: cyclic venting without cleaning (red), and cyclic venting after 3 different cleaning methods (data from METAS).

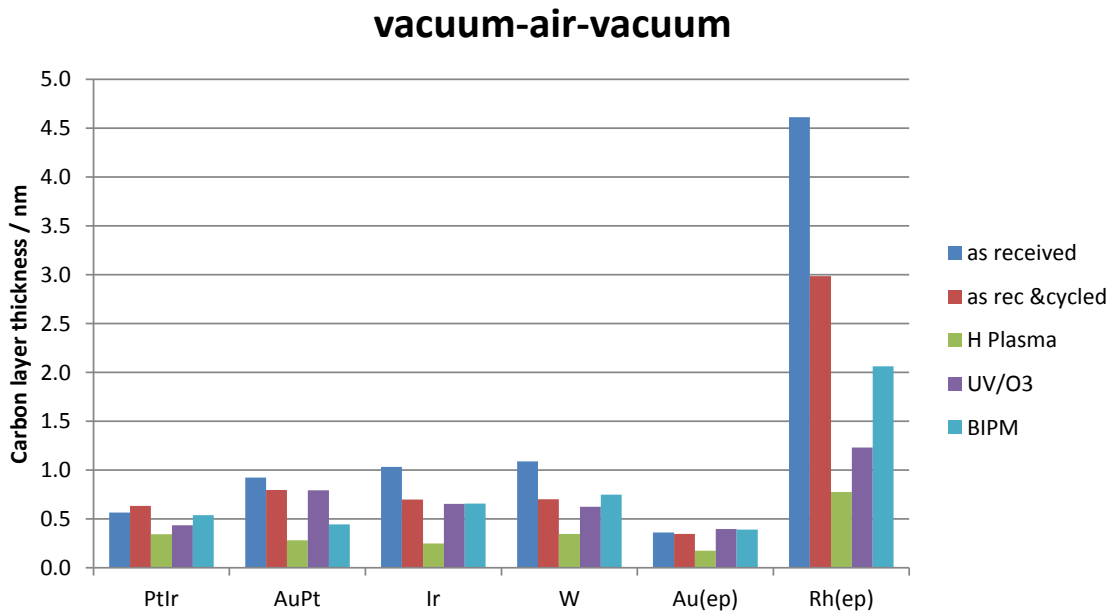


Figure 3b: Final carbon layer thickness for different materials as received and after cyclic venting directly to air for different initial conditions: cyclic venting without cleaning (red), and cyclic venting after 3 different cleaning methods (data from METAS).

| | PtIr | | AuPt | | Ir | | W | | Au(ep) | | Rh(ep) | |
|---|---|---|---|---|---|---|---|---|---|---|---|---|
| **1** | H Plasma | 0.343 | H Plasma | 0.282 | H Plasma | 0.248 | H Plasma | 0.347 | H Plasma | 0.176 | H Plasma | 0.776 |
| **2** | UV/O3 | 0.436 | BIPM | 0.444 | BIPM | 0.546 | UV/O3 | 0.624 | as rec &cycled | 0.348 | UV/O3 | 1.663 |
| **3** | BIPM | 0.509 | UV/O3 | 0.792 | UV/O3 | 0.555 | as rec &cycled | 0.703 | as re-ceived | 0.362 | BIPM | 2.062 |
| **4** | as re-ceived | 0.565 | as rec &cycled | 0.796 | as rec &cycled | 0.700 | BIPM | 0.748 | BIPM | 0.391 | as rec &cycled | 2.985 |
| **5** | as rec &cycled | 0.633 | as re-ceived | 0.923 | as re-ceived | 1.034 | as re-ceived | 1.091 | UV/O3 | 0.408 | as re-ceived | 4.611 |

Table 3: Ranking list of best processes on the basis of hydrocarbon contamination for 6 materials. Listed are the calculated overlayer thicknesses of carbon in nanometre (data from METAS).

| | As received | | as rec &cycled | | H Plasma | | UV/O3 | | BIPM | |
|---|---|---|---|---|---|---|---|---|---|---|
| **1** | Au(ep) | 0.362 | Au(ep) | 0.348 | Au(ep) | 0.176 | Au(ep) | 0.408 | Au(ep) | 0.391 |
| **2** | PtIr | 0.565 | PtIr | 0.633 | Ir | 0.248 | PtIr | 0.436 | AuPt | 0.444 |
| **3** | AuPt | 0.923 | Ir | 0.700 | AuPt | 0.282 | Ir | 0.555 | PtIr | 0.509 |
| **4** | Ir | 1.034 | W | 0.703 | PtIr | 0.343 | W | 0.624 | Ir | 0.546 |
| **5** | W | 1.091 | AuPt | 0.796 | W | 0.347 | AuPt | 0.792 | W | 0.748 |
| **6** | Rh(ep) | 4.611 | Rh(ep) | 2.985 | Rh(ep) | 0.776 | Rh(ep) | 1.663 | Rh(ep) | 2.062 |

Table 4: Ranking list of materials on the basis of hydrocarbon contamination for the different processes applied. Listed are the calculated overlayer thicknesses of carbon in nanometre (data from METAS).

Regarding the cleaning procedures, both the residual contamination right after cleaning and the saturation level after cyclic venting is lowest for hydrogen plasma at METAS, but the relative increase of the recontamination upon cyclic venting is largest. UV/ozone and the nettoyage-lavage procedure show variable results. For most materials the level of contamination is comparable low except for Rh where it is much higher. In contrast, NPL found that the saturation level of recontamination is highest for PtIr after H-plasma (see section 3.3, Figure 8).

In parallel with the samples an Au-coated quartz crystal was exposed to the hydrogen plasma and UV/ozone cleaning and the change in mass on its surface was monitored continuously. The change in layer thickness is depicted in Figure 4 for the H-plasma (left) and for the UV/ozone cleaning (right). During the hydrogen plasma cleaning the overlayer thickness was continuously reduced following an exponential curve. In strong contrast, the overlayer thickness on the UV/ozone cleaned quartz crystal was rapidly increased at first and then decreased. We attribute the increase and the decrease of the overlayer thickness to the accumulation of oxygen and the removal of hydrocarbons, respectively. Previous studies showed that UV/ozone resulted in a rapid oxidation of the gold-coated quartz crystal [7, 8]. In parallel, hydrocarbons were reduced, but much slower, resulting in this changeover of the overlayer thickness. Details of the QCM and the overlayer thickness calculations can be found elsewhere [10].

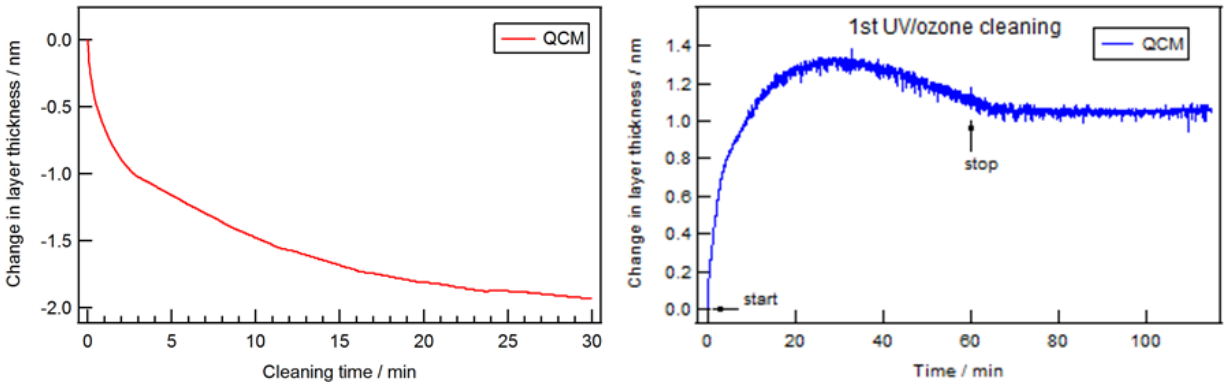


Figure 4: The change in layer thickness during H-plasma and UV/ozone cleaning is recorded by a gold-coated quartz crystal (data from METAS).

## 3.3 Comparison of different venting cycles

Figure 5 shows the increase of the calculated C-contamination layer after H-plasma cleaning as a function of the number of venting cycles using 3 different venting procedures. Right after cleaning, the contamination rate is highest but slows down with increasing number of cycles. The curves are exponential fits to the data. Direct exposure to air shows the fastest and highest recontamination. Venting first with dry nitrogen then followed by exposures to air results finally in the same amount of contamination. Venting exclusively with dry $N_2$ shows the slowest increase in carbon contamination. In contrast to the other venting procedures where saturation is reached after roughly 4 cycles, the hydrocarbon layer keeps on growing. We assume that finally the same level of contamination will be reached, but much more venting cycles are needed. Taking into account the effort for handling and measuring under $N_2$ atmosphere there is no advantage to work under these conditions.

We note that XPS delivers good relative layer thicknesses, but for absolute values a calibration is needed. In the case of not layer-by-layer growth (e.g. islands formation) the thickness values represent the amount of substance or concentration rather than the actual thickness.

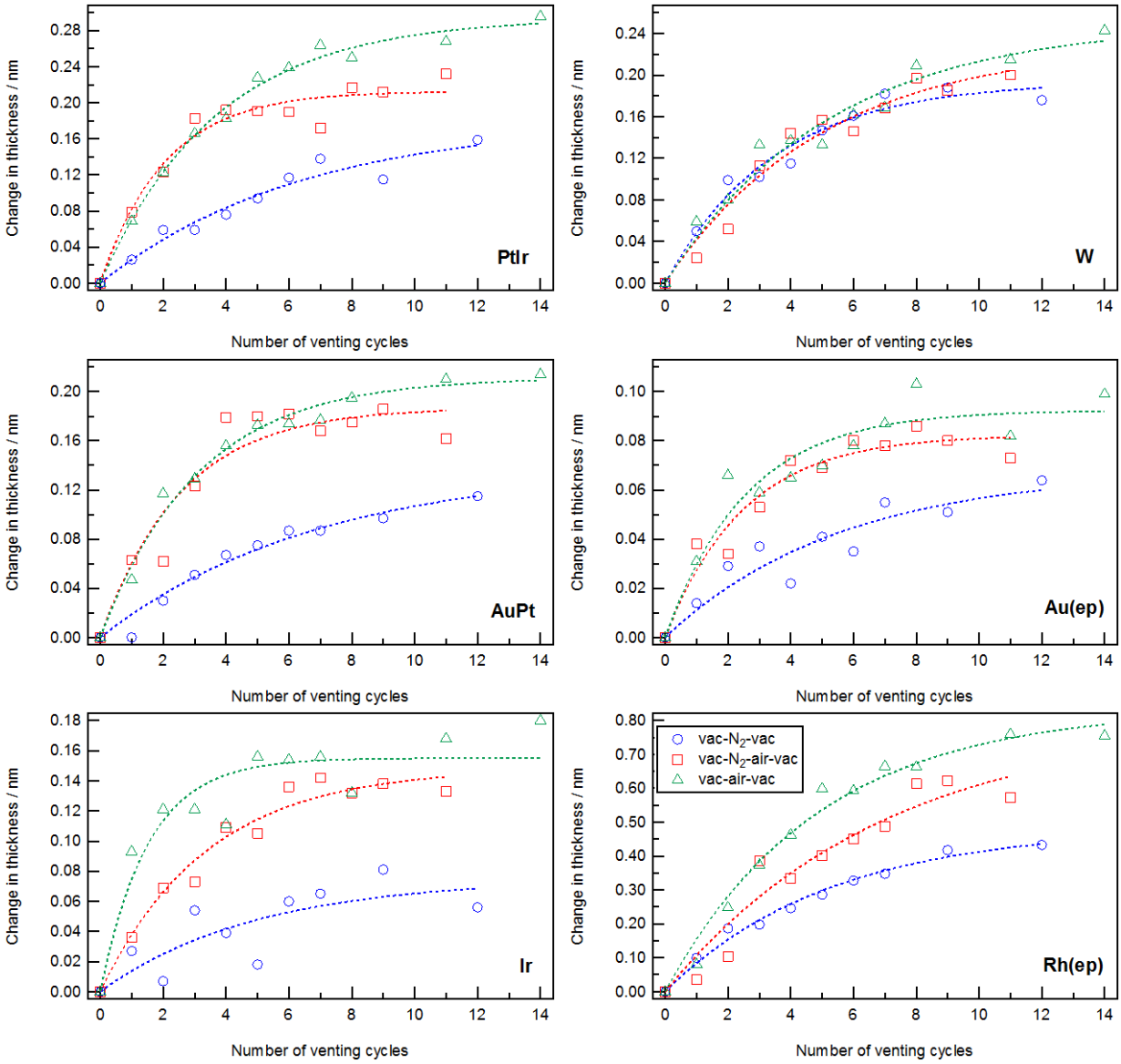


Figure 5: Change in carbon layer thickness after H-plasma cleaning as a function of the number of venting cycles for 3 different venting procedures and for 6 different materials (data from METAS).

By means of the QCM the change in surface layer thickness during the transition between stable environment conditions such as vacuum and ambient pressure nitrogen or air was monitored directly and continuously. The gain in mass monitored with the QCM for different venting procedures is depicted in Figure 6. The overlayer first grows very rapidly but slows down exponentially. For subsequent venting cycles, the growth is linear but small. Venting with dry nitrogen exclusively results in a slightly smaller layer thickness than venting with air or $N_2$ and air.

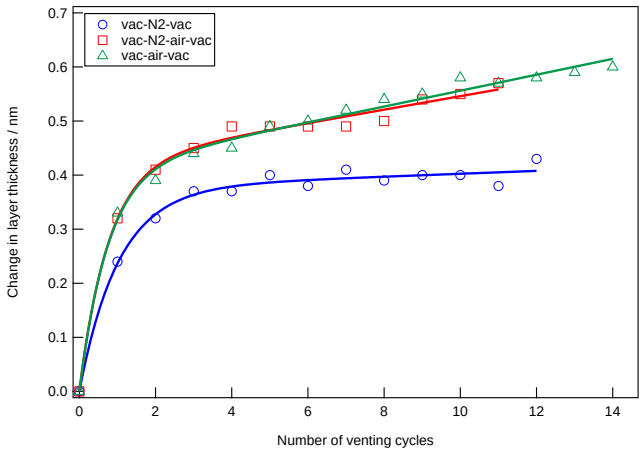


Figure 6: Irreversible gain in mass for different venting procedures after H-plasma cleaning (data from METAS).

The sorption and desorption is depicted in Figure 7. After the formation of an initial hydrocarbon layer during the first 3-4 cycles both sorption and desorption are equal and remain constant. For both exposures to air the sorption is twice as much as for venting with $N_2$ only. This indicates that in air the sorption is caused by water and atmospheric gases, while in nitrogen only the surrounding gas is adsorbed. The difference between sorption and desorption delivers the irreversible contamination rate per cycle; after the 4$^{th}$ venting cycle the contamination rate is very small and constant.

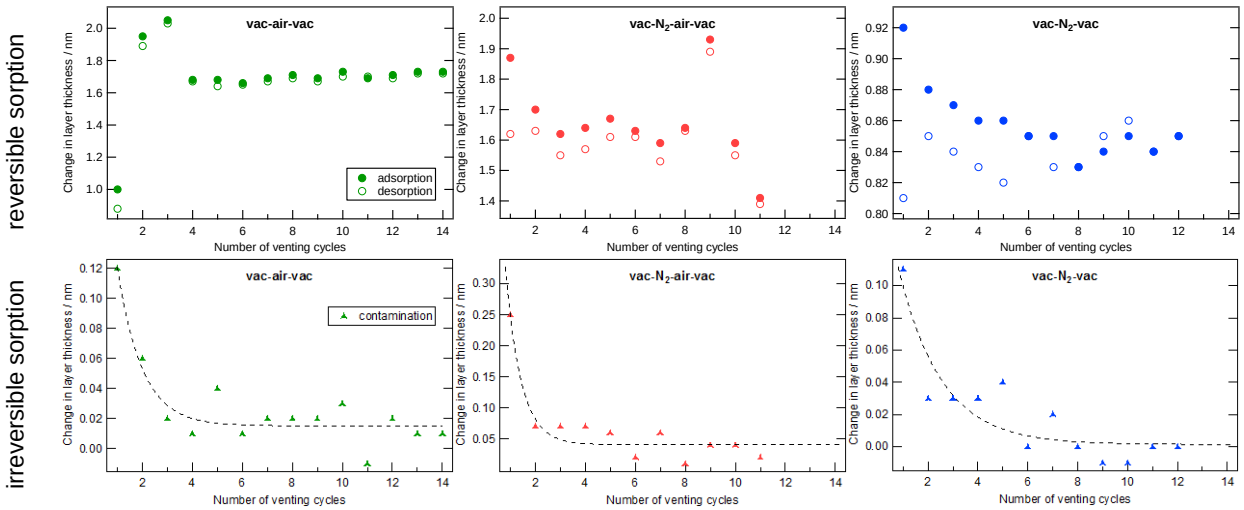


Figure 7: Sorption and desorption for different venting cycles (top) and the irreversible gain in mass per cycle (bottom) (data from METAS).

Figure 8 summarizes the results from NPL on 3 different venting cycles after 3 different cleaning procedures for PtIr and Si.

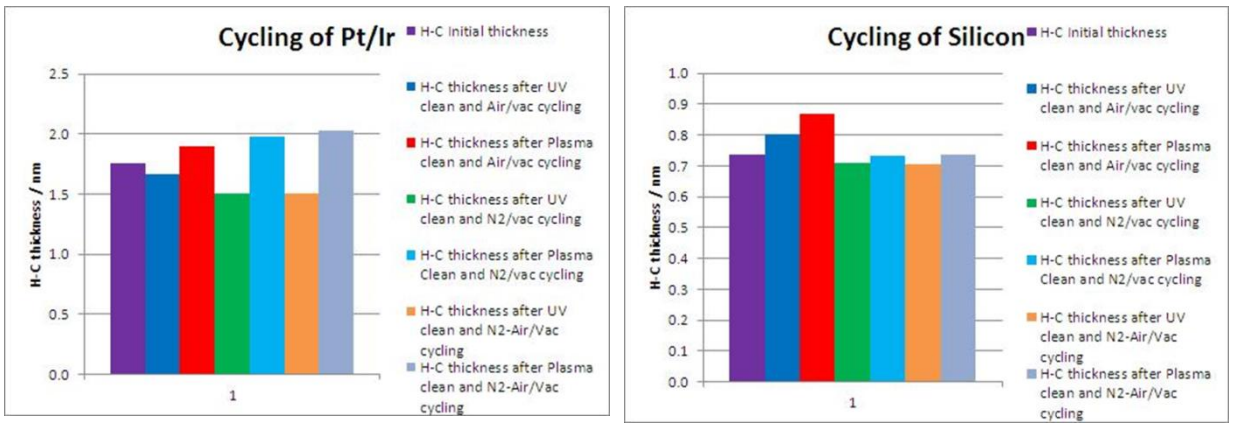


Figure 8: Contamination layer thicknesses after UV/ozone and H-plasma cleaning for different venting cycles (data from NPL).

The silicon samples cycled between air and vacuum showed a slight increase in hydrocarbon thickness of 0.1 nm to 0.2 nm compared with the hydrocarbon thickness after cleaning. The silicon samples that were cycled between $N_2$ and vacuum and from $N_2$ to air to vacuum showed no increase in hydrocarbon thickness compared with the thickness after UV/ozone or H-plasma cleaning. In contrast the Pt/Ir samples showed an increase in hydrocarbon thickness due to the cycling processes compared with the thickness after cleaning of about 0.5 nm for the UV/ozone cleaned samples and about 1 nm for the H-plasma cleaned samples. A similar increase in thickness was observed for all the different cycling methods applied to the Pt/Ir samples and the H-plasma cleaned Pt/Ir samples increased in thickness more than the UV/ozone cleaned samples.

The comparison of the final contamination reveals only minor differences between the different venting cycles and cleaning procedures. The contamination level of PtIr is more than twice as much as for silicon.

For PtIr CNAM compared results after cleaning by TDS and by the nettoyage-lavage procedure and after different venting cycles. As an example the total pressure curve with rising surface temperature is shown in Figure 9. The desorption is highest for the initial contaminated surface. After the nettoyage-lavage procedure the desorption is still much higher than for samples cycled between vacuum and air or nitrogen following TDS cleaning. To compare the cycling methods the area under the desorption curve was calculated. Figure 10 shows the global desorption rate for each cycling. Venting cycles from vacuum to nitrogen exhibit the lowest contamination. Surprisingly, exposure directly to air results in a lower contamination than the vacuum-$N_2$-air procedure.

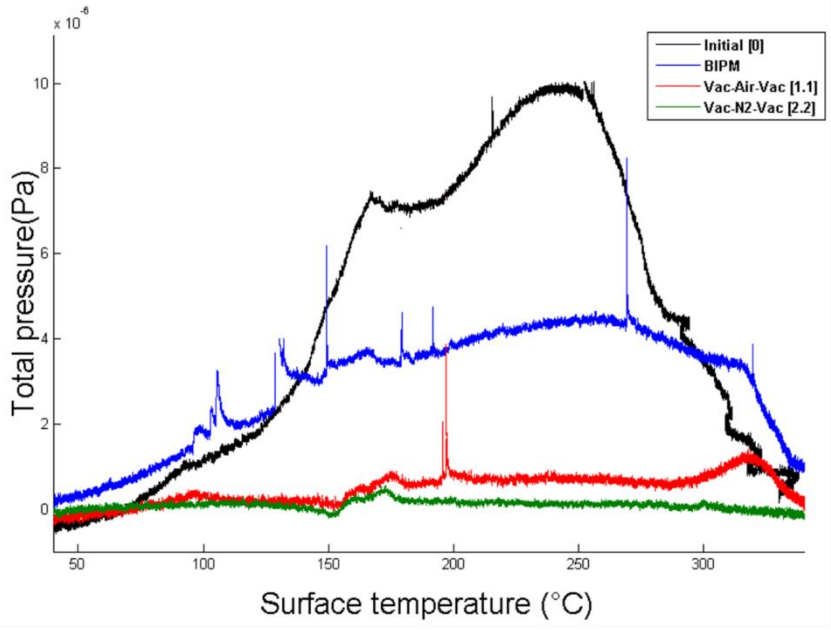


Figure 9: Total pressure versus surface temperature (data from CNAM).

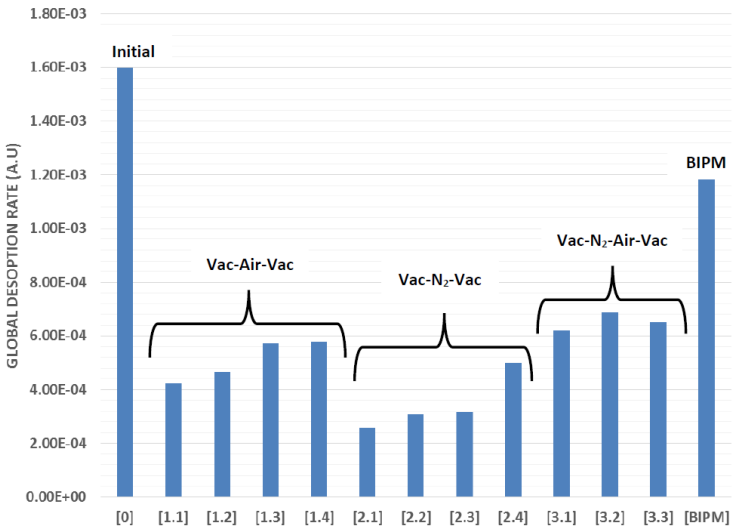


Figure 10: Global desorption rate for each cycling transfer (data from CNAM).

In addition, CNAM performed cyclic venting with vacuum-air-vacuum and vacuum-$N_2$-vacuum on pure Ir and Au-Pt-Ag-Cu artefacts following TDS analysis. Both artefacts showed that vacuum-N2-vacuum resulted in the lowest desorption rate. The findings are in good agreement with the results of the PtIr artefact.

TUBITAK studied the venting processes vacuum-$N_2$-vacuum and vacuum-$N_2$-air-vacuum using two sets of samples for each process. The samples consisted of stainless steel, Ni-alloy, electroplated Au and electroplated Rh. Before and after cycling, the surface chemical state of all samples was analysed by XPS. The results showed that both venting processes caused a decrease of the C 1s intensity on all samples. On the other hand, the intensities of the metals increased for all samples after vacuum-$N_2$-vacuum. But after vacuum-$N_2$-air-vacuum, the intensities of the metals increased for stainless steel, Ni-alloy and electroplated Au, but remained unchanged for electroplated Rh. The results are shown in Figure 11.


Figure 11: Percentile comparison of initial (left) and final (right) surface composition on stainless steel, Ni-alloy, electroplated Au and electroplated Rh for the venting processes vacuum-$N_2$-vacuum and vacuum-$N_2$-air-vacuum (data from TUBITAK).

## 3.4 Dynamic changes / Correlation between pressure and layer thickness

During the venting procedure the pressure and the contamination layer thickness were continuously monitored by means of a compact full range pressure gauge and a quartz crystal microbalance (QCM). The pressure gauge consists of a Pirani sensor for the upper pressure range and a cold cathode magnetron for the high and ultrahigh vacuum. The pressure monitor switches automatically from the Pirani to the cold cathode sensor when going from ambient to vacuum. Figure 12 shows the correlation between pressure and total contamination layer thickness, including recontamination by hydrocarbons as well as water sorption.

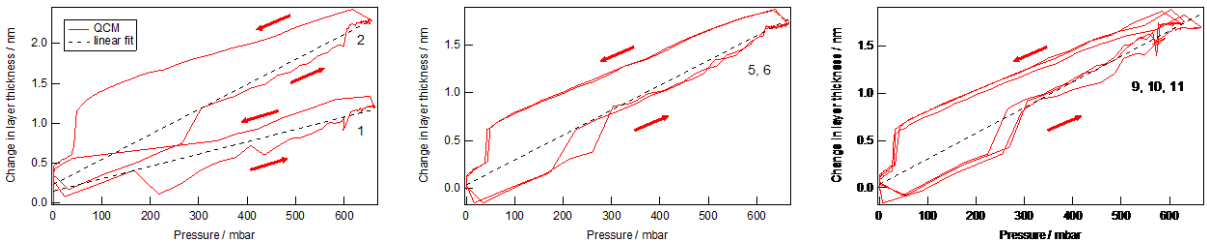


Figure 12: Correlation between pressure and contamination layer thickness (data from METAS).

During the first 4 venting cycles the correlation between layer thickness and pressure changed but remained constant for further cycles. Since the layer thickness is a reaction to the pressure the curve shows a hysteresis between venting and pumping. The kinks at 30 and 250 mbar are due to the automatic switching of the pressure sensors. Besides these kinks the thickness to pressure relation is linear, indicating that these reversible changes are sorbed water. This corresponds to an adsorption according to the BET theory, where in the equilibrium state the adsorption layer thickness is linear with pressure.

# 4 Conclusions

We note that differences between the participating laboratories appeared. The reason for these discrepancies may result from differences in the procedures of the laboratories and locations, e.g. cleaning intensities or time elapsed between processes and surface analysis. However, keeping this in mind some recommendations and conclusions can be drawn.

## 4.1 Sample preparation

The individual results from the participants revealed some contamination mainly by Cu and Ni. The sources of contamination are not clear; consequently, attention is required during all steps of manufacturing, especially the final polishing. The presence of Cu-alloys in the proximity of the standards should be avoided, especially during the final polishing process where polishing liquids are used. Cu can be transported from Cu-alloys via the polishing liquid to the standards as experienced in the Avogadro-project.

## 4.2 Materials

With respect to the recontamination the materials in test show quite similar amounts of contaminants except for Rh where the contamination is initially, as well as after cleaning and cycling, significantly higher.

For most materials except for Rh the final level of contamination is comparable. The speed of recontamination depends on the initial cleanliness. After the formation of a first layer of contaminants further contamination is very small.

From a direct comparison of the different materials at METAS (Table 4) we found electroplated Au and PtIr are top scored for most processes, followed closely by AuPt, Ir and W. Taking into account the results from NPL (e.g. WP3 and WP4) a cross link to other materials can be drawn based on the amount of contamination by hydrocarbons after cyclic venting.

| Rank | Materials |
|---|---|
| 1 | Au (ep), PtIr, Si, Ni-alloy |
| 2 | AuPt, Ir, SS |
| 3 | W |
| 4 | Rh(ep) |

Table 5: Ranking list of best materials tested at all participating laboratories.

## 4.3 Cleaning procedures

The cleaning procedures are content of WP4 and will be discussed there in more detail. We summarize here only results on cleaning procedures obtained in the context of recontamination by cyclic venting. The aim of cleaning is to reach repeatedly reproducible initial surface conditions. After cleaning, the surfaces are rapidly contaminated by hydrocarbons due to cyclic or long term exposure to ambient air. The contamination almost saturates after 3 to 4 weeks or 3-4 venting cycles. The rapid recontamination is almost impossible to avoid, even in dry $N_2$, although the recontamination is slower. Further contamination is rather small. These are the most stable surface conditions. Consequently, acclimatization at ambient pressure for 3 to 4 weeks after cleaning is highly recommended before using the artefacts as mass standards.

At METAS H-plasma resulted in the cleanest surfaces for all tested materials, followed by UV/ozone and nettoyage-lavage. For some materials, e.g. electroplated Au, UV/ozone provokes an oxidation of the metal surface which affects the stability of the samples. The nettoyage-lavage procedure shows the widest spread of results; the reproducibility of this method depends on the operator and is questionable.

The results from NPL show only little differences in the efficiency between UV/ozone and H-plasma, but both being superior to nettoyage-lavage. CNAM demonstrated that also TDS is an effective cleaning compared to the nettoyage-lavage procedure.

| Cleaning procedure | Advantage | Disadvantage |
|---|---|---|
| H-plasma | Repeatable, parameterized, best cleaning at METAS. | Explosive. |
| UV/ozone | Repeatable, parameterized, best cleaning at NPL. | Enhanced oxidation.<br>Hg containing UV lamps.<br>Lamps need to be close to the surface of weights.<br>Can be time consuming. |
| TDS | Repeatable, parameterized. | High temperatures are required.<br>Difficult to apply to large objects ( >1 kg) |
| Nettoyage-lavage | Well-known and established. | Depends on the operator.<br>Cannot be parameterized.<br>Reproducibility is questionable. |

Table 6: Overview of the cleaning methods and their advantages and disadvantages.

## 4.4 Venting cycles

Venting with nitrogen exclusively exhibits the smallest contamination. The results from METAS indicate that the speed of contamination is lowest, but on a long term the same amount of contamination is reached for all venting cycles.
As demonstrated earlier for long term exposure to air [9], the irreversible formation of the first layer can be described by an exponential function. The mass accumulated with time can be described as:

$$m_1(t) = m_{tot1}(1 - e^{-\frac{t}{\tau}}) \tag{4.1}$$

$$m_1(i) = m_{tot1}(1 - e^{-\frac{i}{n}}) \tag{4.2}$$

$$m_{LT}(t) = const \times t \tag{4.3}$$

$$m_{LT}(i) = const \times i \tag{4.4}$$

Where $m_{tot1}$ is the total mass of the completed first layer and $t$ is the exposure time. Further irreversible contamination is very small and linear with time, $t$, or the number of venting cycles $i$. In the case of cyclic venting the mass increase is an exponential function of the number of cycles $i$. The number of cycles to build up the first layer is roughly 4 when cycling to air or nitrogen-air, but much higher (~15 cycles) when cycling to dry nitrogen only. Taking into account the enhanced effort for handling and conducting measurements under nitrogen atmosphere there is no advantage to use this procedure. Venting first with dry nitrogen followed by exposure to air has no advantage (METAS) or is even worse (NPL, CNAM) when compared with direct exposure to air.

| Venting procedure | Comments |
|---|---|
| Vacuum-air-vacuum | Most simple procedure. |
| Vacuum-nitrogen-air-vacuum | No advantage or worse than vacuum-air-vacuum. |
| Vacuum-nitrogen-vacuum | Smallest contamination (NPL, CNAM).<br>Smallest contamination rate, but the same contamination level on a long term (METAS).<br>High effort for handling and conducting measurements under nitrogen atmosphere. |

Table 7: Overview of the different venting methods and their advantages and disadvantages.

## 4.5 Dynamic processes: reversible sorption / desorption

Right after cleaning by H-plasma, a first layer of H-C compounds is formed very rapidly with cyclic exposure to ambient pressure as described in the previous section. During the first 4 cycles the sorption of water and residual gases and the pressure to layer thickness ratio exhibits some irregularities. When the first layer is complete, further contamination is very small and sorption-desorption upon venting cycles remains quite constant. The reversible layer formed by exposure to air is twice as thick as when exposed to ambient pressure dry nitrogen. The reversible layer thickness is proportional to the pressure, indicating that this is a BET type of adsorption.

$$m(p) = const \times p \tag{4.5}$$

The total amount of mass accumulated on the surface can be described as a function of time and pressure:

$$m(t,p) = m_{tot1}\left(1 - e^{-\frac{t}{\tau}}\right) + const \times t + const \times p \tag{4.6}$$

For cyclic processes the time can be replaced by the number of cycles.

## References


[1] Andreas B et al. 2011 Determination of the Avogadro Constant by Counting the Atoms in a $^{28}$Si Crystal *Phys. Rev. Lett.***106** 030801-1-4

[2] Andreas B et al.2011 Counting the atoms in a $^{28}$Si crystal for a new kilogram definition *Metrologia* **48** S1-13

[3] Busch I et al.2011 Surface layer determination for the Si spheres of the Avogadro project *Metrologia* **48** S62-82

[4] Girard G 1990 The washing and cleaning of kilogram prototypes at the BIPM *BIPM Iternal Report*

[5] Smith G C 2005 Evaluation of a simple correction for hydrocarbon contamination layer in quantitative surface analysis by XPS *Journal of Electron Spectroscopy and Related Phenomena* **148** 21 – 28

[6] Seah M P and Spencer S J 2011 Attenuation lengths in organic materials *Surf. Interface Anal.* **43** 744 – 751

[7] Marti K, Fuchs P and Russi S 2012 Cleaning of mass standards: a comparison of new and old techniques *Metrologia* **49** 628-634

[8] Marti K, Fuchs P and Russi S 2013 Cleaning of Mass Standards II: a Comparison of new Techniques applied to new and old Materials *Metrologia* **50** 83-92

[9] Fuchs P, Marti K and Russi S 2012 New instrument for the study of “the kg mise en pratiques”: first results on the correlation between the change in mass and surface chemical state *Metrologia* **49** 607-14

[10] XTC/3 Thin Film Deposition Controller, INFICON.